

Review of Progress in
QUANTITATIVE
NONDESTRUCTIVE
EVALUATION

Volume 5B

Review of Progress in

QUANTITATIVE NONDESTRUCTIVE EVALUATION

Volume 5B

Edited by

Donald O. Thompson

Ames Laboratory (USDOE)

Iowa State University

Ames, Iowa

and

Dale E. Chimenti

Materials Laboratory

Air Force Wright Aeronautical Laboratories

Wright-Patterson Air Force Base

Dayton, Ohio



PLENUM PRESS • NEW YORK AND LONDON

The Library of Congress has cataloged the first volume of this title as follows:

Review of progress in quantitative nondestructive evaluation – Vol. 1 – – New York:
Plenum Press, 1982–

v.: ill.; 28 cm.

Annual.

Vols. 2– published in 2 pts.: A and B.

Vol. 1– are the Proceedings of the 8th, 1981– Air Force/Defense Advanced
Research Projects Agency Symposium on Quantitative Nondestructive Evaluation.

ISSN 0743-0760 – Review of progress in quantitative nondestructive evaluation.

1. Non-destructive testing – Congresses. I. United States. Air Force. II. United States.
Defense Advanced Research Projects Agency. III. Air Force/Defense Advanced
Research Projects Agency Symposium on Quantitative Nondestructive Evaluation.

TA417.2.R48

620.1'127 – dc19

84-646699

Library of Congress

[8502]

AACR 2 MARC-S

Library of Congress Catalog Card Number 84-646699
ISBN 0-306-42269-7

Second half of the proceedings of the Twelfth Annual Review of
Progress in Quantitative Nondestructive Evaluation,
held June 23–28, 1985, in Williamsburg, Virginia

© 1986 Plenum Press, New York
A Division of Plenum Publishing Corporation
233 Spring Street, New York, N.Y. 10013

All rights reserved

No part of this book may be reproduced, stored in a retrieval system, or transmitted
in any form or by any means, electronic, mechanical, photocopying, microfilming,
recording, or otherwise, without written permission from the Publisher

Printed in the United States of America

VOLUME 5B

CHAPTER 5: ELECTRONIC MATERIALS AND DEVICES

Reliability in Electronics.....	955
Harry Quong	
Review of the Accurate Determination of Oxygen in Silicon.....	957
Li Yuezhen and Wang Qimin	
Measurement of Electronic Effects in Semiconductors.....	963
G. S. Kino and R. G. Stearns	
Solid/Solid Interface Thermal Conduction.....	975
S. Utterback	
Defect Mapping in Semiconductors and Metal Films Using Laser-Induced Thermoreflectance.....	981
D. Guidotti and H. M. van Driel	
X-Ray Diffraction Tools and Techniques for Solid State Devices.....	991
M. Fatemi	

CHAPTER 6: COMPOSITE MATERIALS

Section A: Process Control

Modeling the Curing Process of Thermosetting Resin Matrix Composites.....	1001
Alfred C. Loos	
Advanced Concepts in the Control of Autoclave Cure of Composites.....	1015
R. K. Elsley, W. J. Pardee, M. J. Buckley, F. Cohen-Tenoudji, and K. W. Fertig	
Dynamic Dielectric Analysis: A Nondestructive Cure Process Monitoring Method.....	1029
D. E. Kranbuehl, S. E. Delos, E. C. Yi, and J. T. Mayer	
Microdielectric Sensors for Cure Control and Materials Evaluation.....	1037
D. R. Day	
Application of Spectral Analysis Technique for the Study of Curing Reactions in Epoxy Resins.....	1047
S. I. Rokhlin, K. Lewis, K. F. Graff, and Laszlo Adler	
Measurement of the Degree of Cure in Epoxies with Ultrasonic Velocity.....	1055
William P. Winfree and F. Raymond Parker	
Acoustic Characterization of Composite Cure.....	1063
F. Raymond Parker and William P. Winfree	

Section B: Properties and Defects

Ultrasonic Investigation of Elastic Anisotropy in Carbon Fibre Reinforced Injection Moulded Components.....	1069
J. D. Aindow, R. C. Chivers, M. F. Markham, K. E. Puttick, and J. G. Rider	
Surface Generation and Detection of Coupled Fiber-Matrix Mode Acoustic Wave Propagation in Fiber-Reinforced Composites.....	1077
W. T. Yost and John H. Cantrell	
Leaky Lamb Waves in Fibrous Composites Laminates.....	1083
D. E. Chimenti and Adnan H. Nayfeh	
Nondestructive Evaluation of Composite Materials Using Acoustic Microscopy.....	1093
B. T. Khuri-Yakub, P. Reinholdtsen, and J. L. Arnaud	
Evaluation of Damage in Composite Materials by Means of Internal Friction and Young's Modulus.....	1099
K. Matsushita, S. Nishijima, K. Suganuma, T. Okada, and T. Okamoto	
A Model for Eddy-Current Interactions with Advanced Composites.....	1105
Thomas M. Roberts and Harold A. Sabbagh	
Probe Properties Affecting the Eddy Current NDI of Graphite Epoxy.....	1113
Susan N. Vernon	
Quantitative Thermal Diffusivity Measurements of Composites.....	1125
D. Michele Heath, Christopher S. Welch, William P. Winfree, Joseph S. Heyman, and William E. Miller	
Quantitative Thermal Characterization of Thin Plates.....	1133
Christopher S. Welch, D. Michele Heath, and William P. Winfree	
Nondestructive Evaluation of a Carbon Fiber Composite Using the Mirage Effect.....	1141
L. J. Inglehart, F. Lepoutre, F. Charbonnier, and D. Fournier	
Nondestructive Evaluation of Composite Materials by Pulsed Time Domain Methods in Imbedded Optical Fibers.....	1149
R. O. Claus, K. D. Bennett, and B. S. Jackson	
Some Ultrasonic Characteristics of Silicon Carbide Whisker and Particulate Reinforced Aluminum Alloy Composites.....	1157
Philip L. Blue	

Application of Noncontacting Electromagnetic Acoustic Transducers (EMATs) for the Characterization of the Temperature Dependent Elastic Properties of Gr/Al Metal Matrix Composites.....	1163
John M. Liu	

Electrical Conductivity in Heat Treated Aluminum Alloys Reinforced with Discontinuous Silicon Carbide Whiskers.....	1171
John M. Liu and Susan N. Vernon	

Section C: Defects

Backscattering from Flaw Distributions in Composite Materials.....	1179
J. D. Achenbach and J. Qu	
Backscatter B-Scan Images of Defects in Composites.....	1189
Richard W. Martin and Robert J. Andrews	
Nondestructive Evaluation of Composite Laminates by Leaky Lamb Waves.....	1199
Y. Bar-Cohen and D. E. Chimenti	
Detection of Fiber Damage in a Graphite Epoxy Composite Using Current Injection and Magnetic Field Mapping.....	1207
Travis N. Blalock and William T. Yost	
Hidden Impact Damage in Thick Composites.....	1215
C. C. Poe, Jr., W. Illg, and D. P. Garber	
Correlation of Ultrasonic Polar Backscatter with the Depty Technique for Assessment of Impact Damage in Composite Laminates.....	1227
Earl D. Blodgett, J. G. Miller, and S. M. Freeman	
Correlation of the Depty Technique with Ultrasonic Imaging of Impact Damage in Graphite/Epoxy Composites.....	1239
B. T. Smith, J. S. Heyman, J. G. Moore, S. J. Cucura, and S. M. Freeman	
Thermographic NDE of Impact-Induced Damage in Fiber Composite Laminates.....	1245
M. G. Mirchandani and Philip V. McLaughlin, Jr.	
Nondestructive Inspection of Composite Structures by Low-Velocity Impact.....	1253
R. D. Adams, A. M. Allen, and P. Cawley	
Production of Controlled Porosity Specimens for Ultrasonic Evaluation of Composite Structures.....	1259
M. D. Fuller, K. A. Barrett, and R. S. Kiwak	
Effects of Porosity on Polar Backscatter from Fiber Reinforced Composites.....	1267
Earl D. Blodgett, Lewis J. Thomas III, and J. G. Miller	
Variations in Ultrasonic Backscatter Attributed to Porosity.....	1275
D. E. Yuhas, C. L. Vorres, and Ron Roberts	

CHAPTER 7: MATERIALS CHARACTERIZATION

Section A: Properties

Elastic Wave Propagation Through the Interface Between Two Generally Anisotropic Materials.....	1285
S. I. Rokhlin, Ken Bolland, and Laszlo Adler	
An Application of the Rayleigh Wave to the Study of Metal-Electrolyte Interface.....	1293
Ellina Lunarska and Andrzej Zielinski	
Interface Properties Characterization by Interface and Lamb Waves.....	1301
S. I. Rokhlin	
Ultrasonic Analysis of Thin Adhesive Bonds.....	1309
Chris A. Pickett	
Ultrasonic Verification of Microstructural Changes Due to Heat Treatment.....	1315
Edward R. Generazio	
Morphological Investigation of Ultrasonic Techniques for Materials Evaluation.....	1327
Chandra S. Vikram and Clay Olaf Ruud	
Microstructural Characterization of Polycrystalline Nickel Using Magnetic NDE Methods.....	1335
R. Ranjan, O. Buck, and R. B. Thompson	
Acoustic Emission: An NDE Technique for Characterizing the Martensitic Transformation.....	1345
Y. Berlinsky, M. Rosen, J. A. Simmons, and H. N. G. Wadley	
Ultrasonic Backscatter and Attenuation in Consolidated RSP Powder.....	1355
K. L. Telschow and J. E. Flinn	
Measurement of the Coherent Scattering Contribution to the Ultrasonic Attenuation in Penetrable Media.....	1365
R. C. Chivers, J. Adach, and L. W. Anson	
Internal Friction Method for NDE of New Ceramics.....	1373
K. Matsushita and T. Okamoto	
Mirage Effect Measurement of Thermal Diffusivity.....	1379
R. L. Thomas; L. D. Favro, D. S. Kim, P. K. Kuo, C. B. Reyes, and Shu-Yi Zhang	
Determination of Electrical Conductivity Profiles from Frequency-Sweep Eddy Current Measurements.....	1383
A. H. Kahn, K. R. Long, S. Ryckebusch, T. Hsieh, and L. R. Testardi	

NDT of Nylon Ropes Using Magnetic Resonance Techniques.....	1393
W. A. Bryden and T. O. Poehler	

Section B: Acoustoelasticity and Stress

The Acoustoelastic Response of an Aluminum Plate During Elastic-Plastic Deformation.....	1397
T. Eric Wong and George C. Johnson	
Rayleigh Wave Propagation in Deformed Orthotropic Materials.....	1407
P. P. Delsanto and A. V. Clark, Jr.	
Surface Waves in Anisotropic Materials.....	1415
G. Thomas Mase and George C. Johnson	
Absolute Acoustoelastic Measurements of Stress in Textured Plate with Arbitrary Stress Orientations.....	1423
S. S. Lee, J. F. Smith, and R. B. Thompson	
Acoustoelastic Constants in Dilute Two-Phase Alloys.....	1431
K. Salama, E. Schneider, and S. L. Chu	
Influence of Shear Stresses on the Velocities of Ultrasonic Compressive and Shear Waves.....	1439
Ph. Menu, B. de Halleux, and B. de Meester	
Absolute Ultrasonic Determination of Stresses in Aluminum Alloys.....	1449
Alfred V. Clark, Jr., and John C. Moulder	
Ultrasonic Techniques for Residual Stress Measurement in Thin Welded Aluminum Alloy Plates.....	1461
A. V. Clark, J. C. Moulder, R. E. Trevisan, T. A. Stewart, and R. B. Mignogna	
Measurements of Internal Stress Using Magnetomechanical Damping in the Rayleigh Region.....	1473
D. N. Beshers and V. F. Coronel	
Magnetoacoustic Stress Measurement in Railroad Rail Steel.....	1481
M. Namkung, D. Utrata, S. G. Allison, and J. S. Heyman	
Effect of Texture on Magnetoacoustic Stress Measurement in Steel.....	1489
M. Namkung, D. Utrata, S. G. Allison, and J. S. Heyman	

Section C: Processes

Ultrasonic Characterization of Machining Damage in Ceramics.....	1499
L. Clarke, C-H. Chou, B. T. Khuri-Yakub, and D. B. Marshall	

An Assessment of Various Methods Which Detect Critical Surface Flaws in Sintered SiC.....	1509
W. Friedman, A. R. Bhagat, M. Srinivasan, and J. A. Olson	

Thermal Wave Studies of Coatings and Coated Materials.....	1519
P. K. Kuo, C. B. Reyes, L. D. Favro, R. L. Thomas, D. S. Kim, and Shu-Yi Zhang	

Eddy Current Nondestructive Evaluation of Laser Glazed Metallic Surfaces.....	1525
R. J. Churchill, H. P. Groger, J. M. Glass, and W. Lord	

Enhanced Castings by the Use of Ultrasonics.....	1533
B. R. Tittmann, M. R. Mitchell, M. Abdel-Gawad, and J. Bulau	

Nondestructive Evaluation of Corroded Needles by Mirage Effect.....	1543
L. J. Inglehart, F. Lepoutre, and E. Legal Lasalle	

Electromagnetic Methods to Detect Corrosion in Aircraft Structures.....	1549
S.N. Rowland, G.L. Burkhardt, and A.S. Birring	

Section D: Deformation

An Ultrasonic Method of Detecting the Behavior of Dislocations at High Rates of Strain.....	1557
Jumpei Shioiri, Katsuhiko Satoh, and Kiyotaka Sakino	

Ultrasonic Characterization of Plastic Deformation in Metals.....	1565
S. G. Allison, J. S. Heyman, and K. Salama	

Acoustic Emission Source Characterization of Microcracking in A533B Steel.....	1573
Takanori Ohira and Yih-Hsing Pao	

Ultrasonic Characterization of Fatigue Cracks.....	1583
O. Buck, R. B. Thompson, and D. K. Rehbein	

Ultrasonic Studies of Load Induced Changes in Fatigue Crack Closure.....	1591
D. K. Rehbein, R. B. Thompson, and O. Buck	

Detection of Fatigue Cracks in Cladded Blocks.....	1601
G. P. Singh, R. A. Cervantes, R. C. Manning, and S. Takama	

Section E. Porosity

Effects of Pore Shapes on Low Frequency Wave Speed in Porous Media.....	1609
A. N. Norris	

Kramers-Kronig Relations and the Ultrasonic Characterization of Porosity.....	1617
James H. Rose	

Gas Porosity Evaluation in Cast Aluminum Alloys.....	1625
Dave Rypien, Laszlo Adler, and Dennis Hetzner	

Evaluation of Porosity in Aluminum Alloy Castings by Single-Sided Access Ultrasonic Backscatter.....	1633
D. K. Hsu, D. O. Thompson, and R. B. Thompson	

Relative Effects of Porosity and Grain Size on Ultrasonic Wave Propagation in Iron Compacts.....	1643
R. B. Thompson, W. A. Spitzig, and T. A. Gray	

Detection of Voids in Plastic Concrete in Roadways.....	1655
Frank A. Iddings and James L. Melancon	

Section F. Weldments

Ultrasonic Nondestructive Evaluation of Tube Closure Welds.....	1665
G. H. Thomas, J. R. Spingarn, T. A. Jones, and E. I. DuPont	

Immersion Ultrasonic NDE of Tubing Pinch Welds.....	1671
D. K. Rehbein, D. K. Hsu, R. B. Thompson, and T. A. Jones	

Ultrasonic Analysis of Inertia Welds.....	1681
B. L. Armstrong, S. Meng, L. Adler, and W. A. Baeslack, III	

UT of Austenitic Welds and Cladding Using Electro- magnetically Excited SH-Waves.....	1687
G. Hubschen and H. J. Salzburger	

Elastic Ray Tracing to Measure the Integrity of Complex Welded Structures.....	1697
C. Fiedler, S. Meng, and L. Adler	

Sizing Planar Flaws in Weldments Using Low-Frequency EMATS.....	1705
Raymond E. Schramm and Thomas A. Siewert	

Electric Current Perturbation Method for Inspection of Aluminum Welds.....	1713
Gary L. Burkhardt, Gerald W. Scott, and B. N. Ranganathan	

CHAPTER 8: FEDERAL SCIENCE POLICY AND TECHNOLOGY TRANSFER

Federal Science Policy and Industrial Competitiveness.....	1723
Ora E. Smith	

Commercialization of Technology: Considerations for Successful Transfer.....	1735
G. J. Posakony	

Technology Transfer: An Entrepreneur's Perspective.....	1739
George A. Alers	
University Efforts in the Technology Transfer Process.....	1743
R. Bruce Thompson	
NDE Technology Transfer in Primary Metals--A Case Study.....	1747
P. M. Kasprzyk	
NDE Technology Transfer Within the U.S. DOE Weapons Complex.....	1755
A. R. Willis	
Transition and Transfer of Technology--Panel Session Discussions: A Summary.....	1761
G. J. Posakony	
ATTENDEES.....	1769
CONTRIBUTORS.....	1789
CONTRIBUTORS INDEX.....	1817
SUBJECT INDEX.....	1821

REVIEW OF THE ACCURATE DETERMINATION OF OXYGEN IN SILICON

Li Yuezhen and Wang Qimin

Shanghai Institute of Metallurgy
Academia Sinica
Shanghai, China 200050

INTRODUCTION

One of the important problems in characterizing the quality of single crystal silicon is the determination of its oxygen content. There are many experimental methods for determining the oxygen content in silicon, for example, infrared absorption method, gas-fusion method, α -particle activation analysis and photon activation analysis. Among these methods the ir absorption method is the simplest and is non-destructive. However, the ir absorption method for measuring the oxygen content in silicon must be first calibrated by the other methods. In 1957, Kaiser et al. [1,2] first established the calibration curve for determining the oxygen content in silicon. Baker [3] suggested another calibration curve in 1970, which was in coincidence with the result of ^3He activation analysis by Gross [4]. ASTM adopted Baker's calibration curve as the standard in 1971. This calibration relationship between the ir absorption coefficient and the oxygen concentration has a large uncertainty. Moreover, the calibration constant would be probably high. In 1977, according to Graff's data [5], a standard was proposed in West Germany (DIN), but the calibration constant is much lower than Baker's data. However, Yatsurugi et al. [6] in 1973 obtained another calibration curve, but they paid no attention to it. Owing to the experimental dispersion in the above mentioned literatures, we established two more accurate calibration curves in 1981 [7] and in 1983 [8], one for 300K, the other for 78K, using inert-gas fusion method and α -particle activation analysis for determining oxygen in silicon. Due to the improvements of the specimen preparation and the ir and the gas-fusion technique, our results are better than those in the literature cited. In 1983 Iizuka [9], using α -particle activation analysis and in 1984 Rath [10], using photon activation analysis, respectively recalibrated the ir absorption curve for determining the oxygen content in silicon at 300K. Within the experimental error their results are consistent with our results.

The above mentioned results obtained by various authors are summarized in the following, and a new method for selecting the ir oxygen-free reference sample used in ir absorption difference method is presented. Finally the key points and the precision of our inert-gas fusion experiment as compared with other works are discussed.

COMPARISON OF EXPERIMENTAL RESULTS

300K Ir Oxygen-determining Calibration Curves and Calibration Constants

Baker's calibration curve is shown in Fig. 1. Figure 2 is Graff's calibration curve. It can be seen from Fig. 1 and Fig. 2 that the experimental dispersion is large. Figure 3 shows our result, the precision will be discussed below. Figure 4 shows Iizuka's calibration

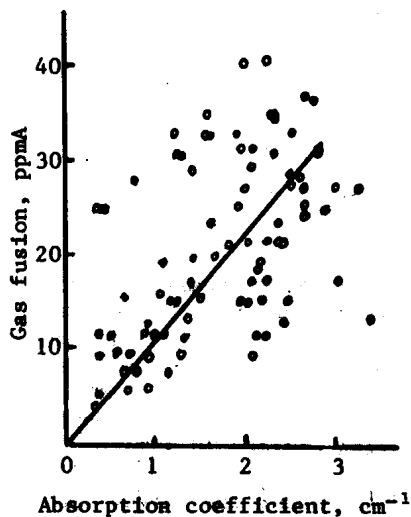


Fig. 1. Baker's calibration curve.

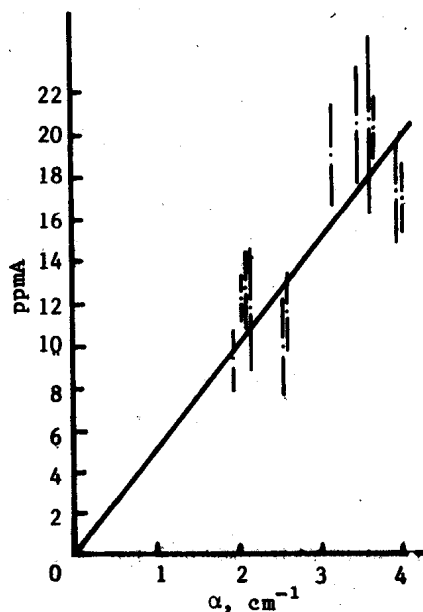


Fig. 2. Graff's calibration curve.

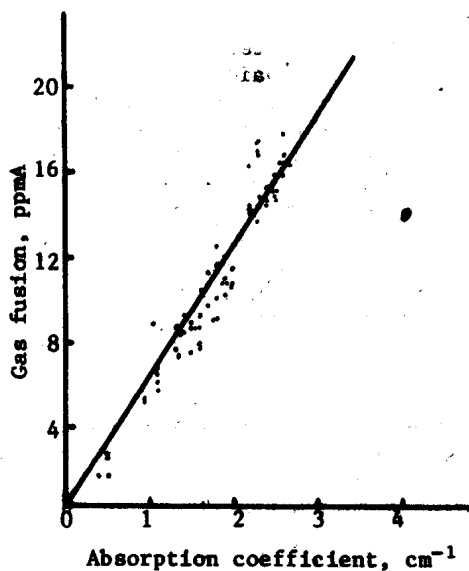


Fig. 3. Our calibration curve.

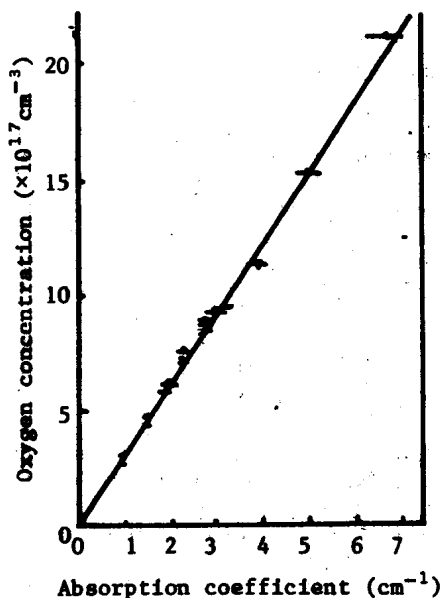


Fig. 4. Iizuka's calibration curve.

curve using α -particle activation analysis and Fig. 5 shows Rath's calibration curve using photon activation analysis. Figure 6 indicates the comparison of the experimental results obtained by various authors. It can be seen that Baker's calibration curve tends toward a high value of oxygen concentration, whereas Graff's calibration curve tends to a low value. Kaiser's result is slightly lower than ours. The calibration curves of Iizuka, Yatsurugi and Rath results are nearby our result. The comparison of calibration constants by various authors is shown in Table I.

Table I. The Comparison of Calibration Constants

Author	Gas analysis ppmA	Absorption coefficient α cm^{-1}	Activation analysis ppmA	Absorption coefficient α cm^{-1}
Baker		9.63 ± 2.29	8.1	
Graff		4.9 ± 0.2	5.9	
Ours		6.2 ± 0.1	6.2 ± 0.4	
Iizuka	}	---	6.06 ± 0.04	
Yatsurugi				
Rath		---	6.0 ± 0.4	

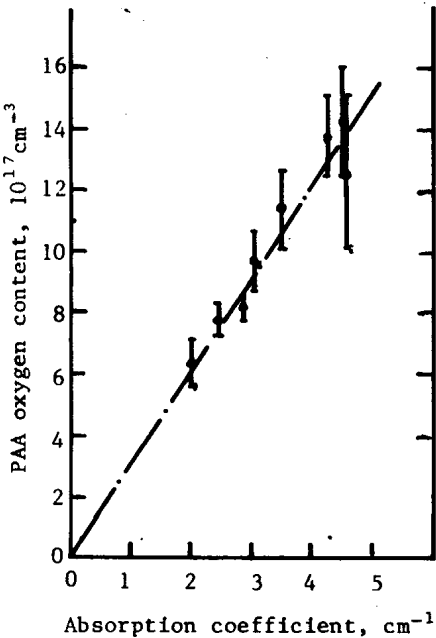


Fig. 5. Rath's calibration curve.

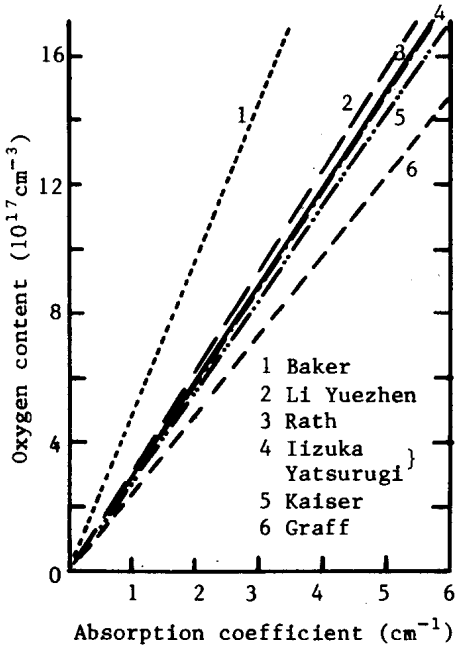


Fig. 6. Comparison of various calibration curves.

78K Ir Oxygen-determining Calibration Curves and Calibration Constants

Because low-temperature measurement can increase the sensitivity (5), the measuring sensitivity of the oxygen content at 80K can be twice that at 300K. Therefore, we carried out the measurements at 78K using ir absorption difference method. ASTM has set a standard that the calibration constant for 78K ir measuring oxygen content is $4.81 \text{ ppmA/cm}^{-1}$ [11,12], but the calibration constant obtained by Graff in 1973 is 1.9 ppmA/cm^{-1} (5). The difference between them is rather large. Figure 7 shows our 78K calibration curve. The calibration constant obtained by us is 2.6 ppmA/cm^{-1} . The comparison of the 78K calibration curves among ASTM, Graff and ours is shown in Fig. 8. From Fig. 7 and Fig. 8, it can be seen that the experimental dispersion in Graff's curve is larger than ours.

A NEW METHOD FOR SELECTING IR OXYGEN-FREE REFERENCE SAMPLE

Using the air-reference method, there is an uncertainty in the absorption coefficient ranging from 0.6 to 1.05 cm^{-1} due to the intrinsic absorption of oxygen in Si-O-Si, whereas in the difference method there is no such uncertainty. Therefore, we have developed a new method for selecting the ir oxygen-free reference sample, which is more convenient, simple and reliable than other methods. This method utilizes the air reference method to measure the ir characteristics of the Si-O-Si absorption band at 78K after which we can distinguish the characteristic absorption of interstitial oxygen from the three photon absorptions of silicon. Thus, the ir oxygen-free sample can be found.

DISCUSSION

The gas-fusion method is a direct method for calibrating the ir absorption coefficient, but it is difficult to control. In order to improve the experimental accuracy, we adopted two procedures: careful preparation of the test specimen and accurate control of the ir and gas-fusion conditions.

Preparation of the Test Specimen

Specimens were prepared as $0.7 \times 0.7 \times 0.5 \text{ cm}$ dice, weighing approximately 0.57 g . They were cut from CZ or FZ n-type and p-type of single

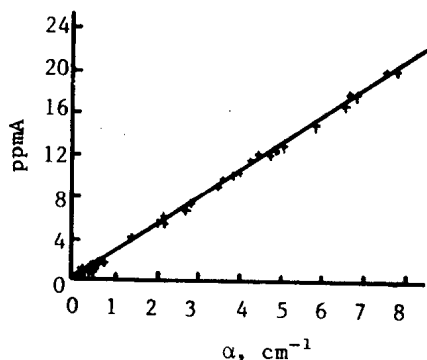


Fig. 7. The relationship between ir absorption coefficient and oxygen content, at 78K.

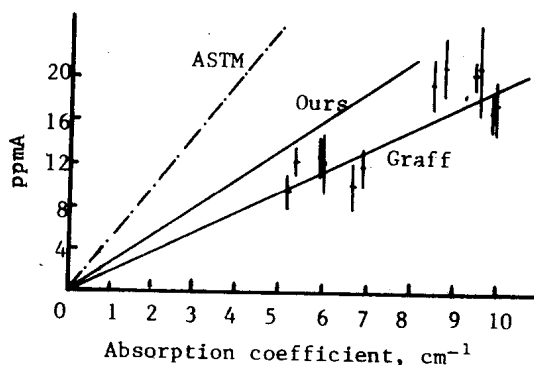


Fig. 8. The comparison among the calibration curves of ASTM, Graff and ours.

crystal silicon <111> orientation. The six faces were carefully polished with syton (colloidal silica) and then the pieces were cleaned by sequential immersion in basic and acidic hydrogen peroxide. Before the inert-gas fusion analysis, each piece was measured by the ir difference method. The area exposed is a circle 5 mm in diameter, thus there is no influence of inhomogeneous distribution of oxygen content. An oxygen content, corresponding to 1.2 ppmA oxygen for each dice, in a surface oxide film of average thickness 14Å was deduced from the gas-fusion result.

Control of the Gas-fusion Condition

We have used the Ni-Sn bath to extract carbon monoxide formed in the reduction process. In order to maintain a stable operating temperature ($1690 \pm 30^\circ\text{C}$), it was necessary to keep the relative positions of the inductive coil and the graphite crucible the same. When the graphite crucible was outgassed sufficiently at 2100°C , the blank of the gas analysis was stable and was reduced to lower than $0.1 \mu\text{g}$.

Comparison of Results

In Fig. 3, 67 pairs of data points from gas-fusion analysis and ir absorption measurement were fitted to the regression line. The calculated value of the calibration constant is 6.2 ppmA, and the correlation coefficient is $r = 0.965$. The standard deviation of the residuals is 1.16 ppmA in our experiment and about 3.85 ppmA in Graff's data. In our diagram, it covers 68% experimental points within the range of $\pm 1.16 \text{ ppmA}$, while in Graff's diagram it covers 68% experimental points in the range of $\pm 3.85 \text{ ppmA}$.

Low temperature (78K) measurement of the ir absorption coefficient can increase the sensitivity of determination and can improve the measuring accuracy, especially for specimens of low oxygen content. Thirty-one data points from the ir difference method at 78K were measured (Fig. 7). Fitting these points by the regression method into a straight line, the calculated value of the calibration constant is $2.59 \text{ ppmA/cm}^{-1}$. The deviation of the slope is 0.19, so that $y = (2.59 \pm 0.19)x$, and the correlation coefficient $r = 0.999$. The residual standard deviation is $s = 0.275 \text{ ppmA}$, while the s of Graff is 2.31. Our diagram (Fig. 7) covers 95% of the experimental points within the range of $\pm 0.55 \text{ ppmA}$, while in Graff's diagram, 95% of the experimental points in the range of $\pm 4.62 \text{ ppmA}$ are included.

Two samples of the high, middle and low oxygen content crystal respectively were chosen for ir measurement at 300K by eight laboratories. The results are that for oxygen concentrations less than 1.15 ppmA the multilaboratory precision (RIS%) is of $\pm 10.1\%$, while for concentrations above 1.15 ppmA the RIS% is of $\pm 6.4\%$, which are better than ASTM results.

CONCLUSION

According to our results, the calibrating formula for 300K is

$$N_{\text{O}} = 3.1 \times 10^{17} \times \alpha \text{ atoms/cm}^3$$

or

$$N_{\text{O}} = 6.2 \times \alpha \text{ ppmA}$$

while that for 78K is

$$N_o = 1.3 \times 10^{17} \times \alpha \text{ atoms/cm}^3$$

or

$$N_o = 2.6 \times \alpha \text{ ppmA}$$

where μ is the ir absorption coefficient.

REFERENCES

1. W. Kaiser, P. H. Keck and C. F. Lange, The Phys. Rev., 101, 1264 (1956).
2. W. Kaiser and P. H. Keck, J. Appl. Phys., 28, 882 (1957).
3. J. A. Baker, Solid-State Electronics, 13, 1431 (1970).
4. C. Grass, et al., J. Electrochem. Soc., 116, 248c (1969).
5. K. Graff, E. Grallath, S. Ades, G. Goldback and G. Tolg, Solid-State Electronics, 16, 887 (1973).
6. Y. Yatsurugi, N. Akiyama, Y. Endo and T. Nozaki, J. Electrochem. Soc., 120, 975 (1973).
7. Li Yuezhen, He Huannan et al., "A New Calibration Curve for Measuring Oxygen Content of Single Crystal Silicon by 9 μ Infrared Absorption Method" Shanghai Institute of Metallurgy, Academy of Sciences of China, May 1981; Li Yuezhen, He Huannan et al., Chinese Journal of Semiconductor 4, 81 (1983); He Huannan, Li Yuezhen, Zhao Guandi, Yan Ronghua, Lu Qingren, Qi Mingwei, Talanta, 30, 761 (1983).
8. Li Yuezhen, Shen Jinyuan and Wang Qimin, Materials Letters, 2, 101 (1983).
9. T. Iizuka, Shin Takasu, M. Tajima, T. Arai, M. Nozaki, N. Tnoue and M. Watanabe, in "Defects in Silicon", The Electrochemical Society, Softbound, Proceedings 83-9, p. 265.
10. H. J. Rath, P. Stallhofer and D. Huber, J. Electrochem. Soc., 131, 120 (1984).
11. 1979 Annual Book of ASTM Standards, Part 43, F121-79.
12. 1981 Annual Book of ASTM Standards, Part 43, F121-80.